

See discussions, stats, and author profiles for this publication at: <https://www.researchgate.net/publication/261606629>

Inhibitor Design Strategy Based on an Enzyme Structural Flexibility: A Case of Bacterial MurD Ligase

ARTICLE in JOURNAL OF CHEMICAL INFORMATION AND MODELING · APRIL 2014

Impact Factor: 3.74 · DOI: 10.1021/ci500104m · Source: PubMed

CITATIONS

5

READS

59

6 AUTHORS, INCLUDING:



[Andrej Perdih](#)

National Institute of Chemistry

44 PUBLICATIONS 440 CITATIONS

[SEE PROFILE](#)



[Martina Hrast](#)

University of Ljubljana

17 PUBLICATIONS 73 CITATIONS

[SEE PROFILE](#)



[Gerhard Wolber](#)

Freie Universität Berlin

145 PUBLICATIONS 2,764 CITATIONS

[SEE PROFILE](#)



[Tom Solmajer](#)

National Institute of Chemistry

98 PUBLICATIONS 1,244 CITATIONS

[SEE PROFILE](#)

Inhibitor Design Strategy Based on an Enzyme Structural Flexibility: A Case of Bacterial MurD Ligase

Andrej Perdih,^{*,†,‡} Martina Hrast,[§] Hélène Barreteau,^{||} Stanislav Gobec,[§] Gerhard Wolber,[‡] and Tom Solmajer[†]

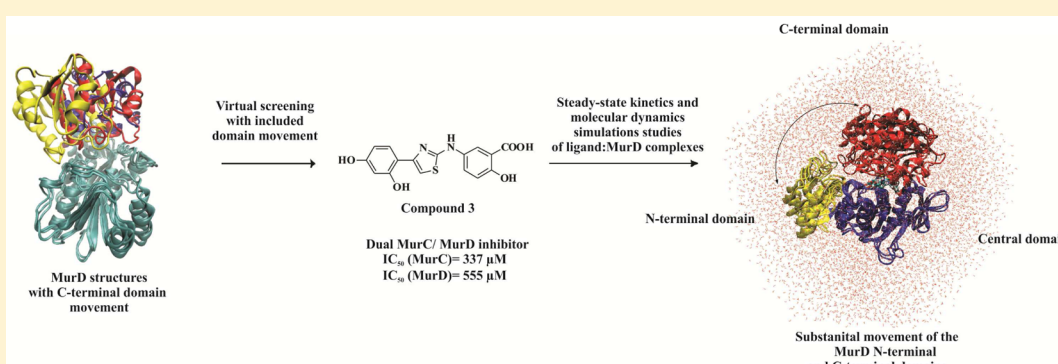
[†]National Institute of Chemistry, Hajdrihova 19, 1001 Ljubljana, Slovenia

[‡]Institute of Pharmacy, Freie Universität Berlin, Königin Luise-Strasse 2 + 4, 14195 Berlin, Germany

[§]Faculty of Pharmacy, University of Ljubljana, Aškerčeva 7, 1001 Ljubljana, Slovenia

^{||}Laboratoire des Enveloppes Bactériennes et Antibiotiques, IBBMC, Université Paris-Sud, 91405 Orsay, France

Supporting Information



ABSTRACT: Increasing bacterial resistance to available antibiotics stimulated the discovery of novel efficacious antibacterial agents. The biosynthesis of the bacterial peptidoglycan, where the MurD enzyme is involved in the intracellular phase of the UDP-MurNAc-pentapeptide formation, represents a collection of highly selective targets for novel antibacterial drug design. In our previous computational studies, the C-terminal domain motion of the MurD ligase was investigated using Targeted Molecular Dynamic (TMD) simulation and the Off-Path Simulation (OPS) technique. In this study, we present a drug design strategy using multiple protein structures for the identification of novel MurD ligase inhibitors. Our main focus was the ATP-binding site of the MurD enzyme. In the first stage, three MurD protein conformations were selected based on the obtained OPS/TMD data as the initial criterion. Subsequently, a two-stage virtual screening approach was utilized combining derived structure-based pharmacophores with molecular docking calculations. Selected compounds were then assayed in the established enzyme binding assays, and compound 3 from the aminothiazole class was discovered to act as a dual MurC/MurD inhibitor in the micromolar range. A steady-state kinetic study was performed on the MurD enzyme to provide further information about the mechanistic aspects of its inhibition. In the final stage, all used conformations of the MurD enzyme with compound 3 were simulated in classical molecular dynamics (MD) simulations providing atomistic insights of the experimental results. Overall, the study depicts several challenges that need to be addressed when trying to hit a flexible moving target such as the presently studied bacterial MurD enzyme and show the possibilities of how computational tools can be proficiently used at all stages of the drug discovery process.

1. INTRODUCTION

Increasing bacterial resistance to most of the available antibiotics has stimulated the discovery of novel efficacious antibacterial agents focusing on previously unexploited targets.^{1–3} A vital component of bacterial cells—bacterial peptidoglycan—is a target of choice with respect to selective toxicity.^{4,5} Peptidoglycan provides the necessary strength for the bacterial cells to withstand the high internal osmotic pressure.^{4,5} The pathway of the bacterial peptidoglycan biosynthesis is a multistage process divided into intracellular assembly of the UDP-MurNAc-pentapeptide, followed by a

translocation phase across the cell membrane and final incorporation into the emerging biopolymer.^{4,5}

Four members of the ADP-forming bacterial ligase family—MurC, MurD, MurE and MurF—are involved in the intracellular steps of the peptidoglycan assembly, catalyzing the synthesis of the peptide moiety by consecutive addition of L-Ala, D-Glu, meso-A₂pm (or L-Lys), and D-Ala-D-Ala to the corresponding UDP precursor.^{4–6} The Mur ligase family

Received: February 18, 2014

Published: April 12, 2014



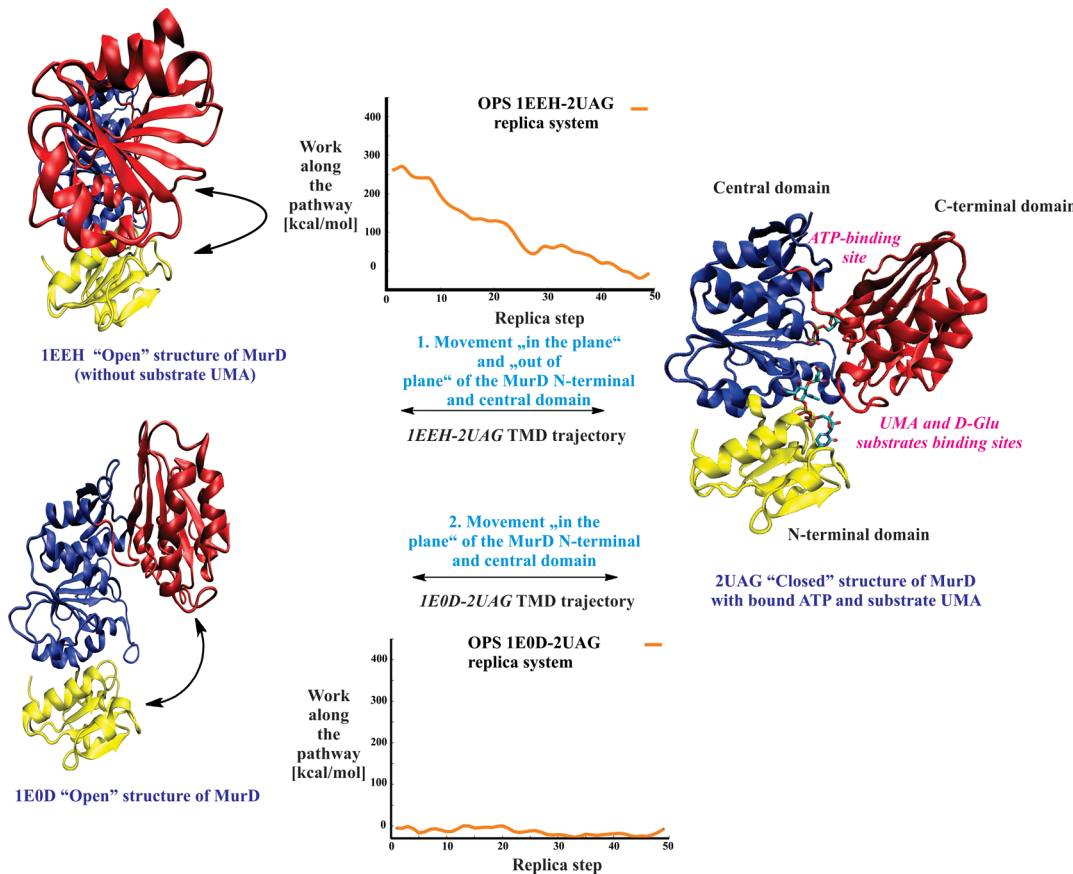


Figure 1. Summary of the performed TMD/OPS studies using experimental MurD protein structures as starting points of our drug design studies.^{13,14} The straight arrows indicate calculated TMD trajectories used in OPS calculations and curved arrows the principal movement from corresponding open to closed MurD structure. The N-terminal domain is colored in yellow, the central domain in blue, and the C-terminal domain in red. (left) The open structure of MurD (1EEH crystal structure) and open structure of MurD (1E0D crystal structure) with the same color scheme. (right) The closed structure of MurD (2UAG crystal structure) with the same color scheme. Calculated OPS energy pathways of the TMD C-terminal domain closing motion of 1EEH–2UAG and 1E0D–2UAG replica systems without included ligands.¹⁴

represents a good example of modular structure in protein architecture, with molecules made up of three domains allowing for specific molecular recognition of each individual UDP substrate.⁶ The three-domain structure of the family comprised the N-terminal domain responsible for binding the UDP substrate, a central domain bearing resemblance to the nucleotide-binding domains of a number of ATP- or GTP-ases, and finally a C-terminal domain, which is involved in the binding of the incoming amino acid or dipeptide.⁶ Structural investigations of the Mur ligase family have resulted in the identification of several distinct conformations of the enzyme, revealing that the whole family encompasses a collection of highly complex dynamic protein targets.⁶

All Mur ligases presumably act through an analogous sequential enzymatic mechanism, as corroborated by structural,⁷ computational,⁸ and biochemical investigations^{9,10} In the proposed mechanism, the bound UDP precursor first reacts with the ATP molecule yielding an acyl-phosphate intermediate,¹¹ which, after the addition of the incoming amino acid (or dipeptide), affords the tetrahedral reaction intermediate.^{4,8–11} Finally, the dissociation of the phosphate group results in a new UDP precursor elongated by the condensed amino acid (or dipeptide).^{7,9,10}

MurD is the second enzyme in the bacterial ligase series and catalyzes a highly specific incorporation of D-glutamate to the cytoplasmic intermediate UDP-N-acetylmuramoyl-L-alanine

(UMA) concomitant with a degradation of ATP to ADP and Pi.⁴ For this enzyme, X-ray structural studies resulted in several MurD crystal structures, providing detailed information regarding the enzyme active conformation as well as the positions and binding patterns of ligands UMA, ADP (PDB: 2UAG and 3UAG), and the product UMAG (PDB: 4UAG).⁷ Further structural X-ray investigations revealed two additional MurD structures, termed “open” structures, where the C-terminal domain undergoes a large rigid-body rotation away from the N-terminal and central domains. These structures, crystallized in the presence (PDB entry: 1EEH) and absence (PDB entry: 1E0D) of the UMA substrate, were found to occupy entirely different positions of the C-terminal domain (Figure 1).¹²

In our ongoing computational exploration of the mechanistic aspects of the MurD ligase, insights into the binding process of UMA and ATP ligands as well as of the conformational transition of the C-terminal domain in the MurD structure at the atomistic level were obtained by exploiting a well-established Targeted Molecular Dynamics (TMD) simulation method (see Materials and Methods section for a detailed description).¹³ The use of the TMD approach yielded 1EEH–2UAG and the 1E0D–2UAG trajectories (Figure 1), with the referred experimental PDB structures acting as boundary structures describing the plausible C-terminal domain closing motion.¹³ Subsequent application of the Off-Path Simulation

(OPS) technique, an extension of the established Replica path method (RPATH), was initiated to provide a relative energy comparison pathway of the two TMD-generated C-terminal domain closing pathways (see Materials and Methods section for a detailed description).¹⁴ The OPS study established much higher energy demands connected with the C-terminal domain closing process commencing from the open structure in which this domain is located out-of plane with respect to the N-terminal and central domains (open structure PDB: 1EEH) in comparison to the open structure in which the conformational movement is confined to this plane (open structure PDB: 1E0D). This is shown on OPS energy graphs presented in Figure 1 for both studied cases of the free enzyme (see also Supporting Information Figure 1S for the OPS energy diagrams of two studied closing TMD motions of the MurD C-terminal domain with included ligands).¹⁴

The MurD enzyme as well as the whole Mur ligase family are widely considered as attractive drug design targets⁴ with many inhibitors already identified.^{15–18} A frequently used starting point in the design of the MurD enzyme inhibitors was the hypothetical structure of the MurD tetrahedral reaction intermediate.¹⁷ From this starting point, a variety of low-molecular-weight analogues of the MurD tetrahedral intermediate structure were discovered, typically classified as derivatives of D-glutamic acid.^{4,18} Subsequent computational studies offered further insights into the molecular recognition process of these inhibitors.^{19,20} At present, ATP-binding sites of all Mur ligases were less frequently utilized in the MurD inhibitor design efforts.²¹ Yet, the structural comparison of the ATP-binding sites within the ligase family suggests that, due to their evident topological and electrostatic uniformity, a unique possibility for concurrent multiple inhibition of the whole ligase chain (MurC–MurF) is possible.⁶ This renders the ATP-binding site as an extremely interesting starting collection of targets for the Mur ligase inhibitor design.⁶

Consideration of the MurD C-terminal domain mobility in the drug design efforts could provide novel ideas and scaffolds of the MurD inhibitors targeting the ATP-binding site. As the MurD enzyme without any ligands was found in an open conformation (PDB structure: 1E0D),¹² and as our TMD/OPS computational studies pointed toward the existence of the equilibrium of available protein structures when the MurD C-terminal domain is located within the central and N-terminal domain,^{13,14} we wanted to include this piece of information about the protein flexibility into account when performing our structure-based drug design experiments. There are indeed already several established cases in the literature where computer-aided drug design campaigns with incorporated protein flexibility (multiple protein structure (MPS) approach) showed considerable utility, especially for proteins that show flexible, dynamic characteristics.^{22–25} Additional evidence of the potential utility within the Mur ligase field is reflected in the reported structural studies of the closely related bacterial MurF ligase from *Streptococcus pneumoniae*. It was demonstrated that inhibitor binding can induce a domain closure, yielding a “closed” conformation of the MurF enzyme, dissimilar to the expected “closed” transition state conformation.²⁶ All of these data inspired us to consider the utilization of the produced TMD/OPS pathways to the MurD structure-based drug design campaigns with incorporated protein flexibility.

In this paper, we demonstrate how TMD/OPS computational studies of the MurD ligase C-terminal domain closing motion could be coupled with a classical computational drug

design procedure in the search for novel MurD ligase inhibitors. We focused primarily on the ATP-binding site of the MurD enzyme. The outline of the design computational platform is depicted in Figure 2. In the first stage, three protein MurD

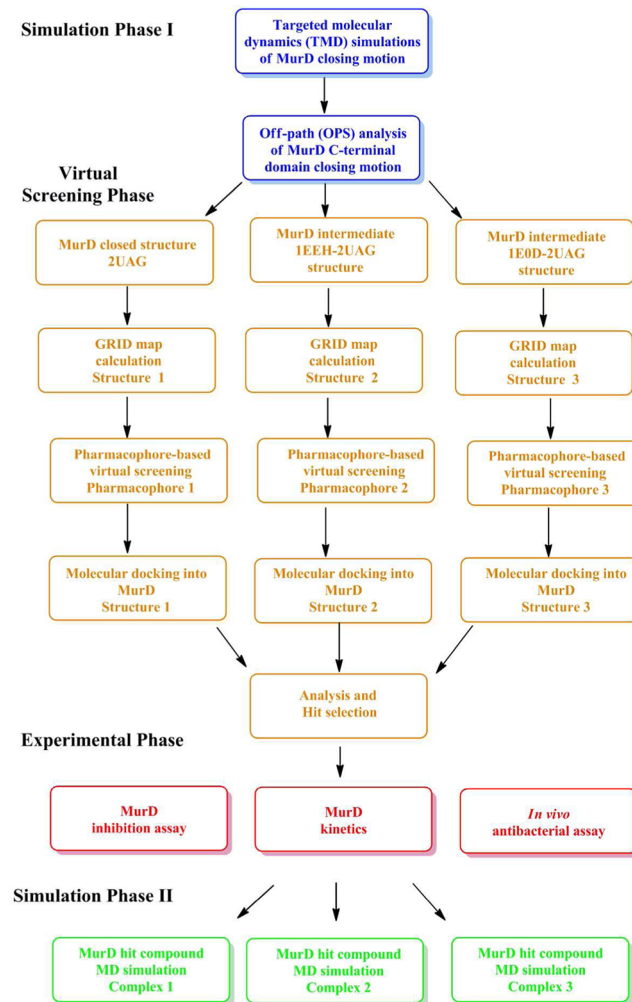


Figure 2. Outline of the designed computational platform of the design of novel MurD inhibitors targeting the ATP-binding site with MurD protein flexibility taken into account.

conformations were selected using the OPS/TMD simulation data as the initial criterion, and GRID maps were calculated for the hot spot identification in the ATP-binding site of these conformations. Subsequently, a two-stage virtual screening approach was utilized combining derived structure-based pharmacophores of the ATP molecule in the selected multiple MurD conformations with molecular docking calculations of the obtained hits into these structures. Selected compounds were then assayed in established enzyme-binding assays, and a steady-state kinetics study was performed versus ATP concentration on the MurD enzyme. In the final stage of this study, conformations of the MurD enzyme with the bound identified active ligand were simulated in molecular dynamics (MD) simulations to provide further insight and rationale of the obtained experimental results. Our study thus demonstrates the challenges, strategies, and pitfalls that need to be addressed when trying to inhibit a flexible moving target^{22,23} such as the MurD bacterial enzyme.

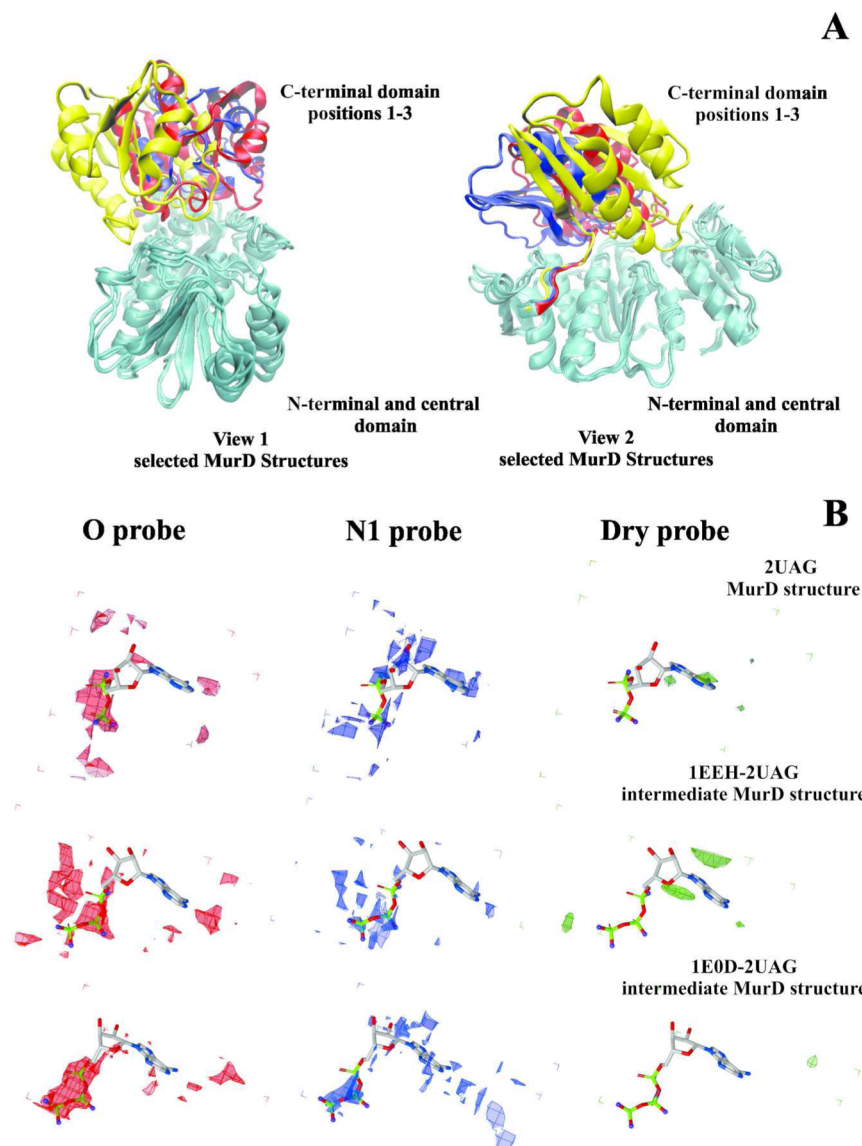


Figure 3. (A) Two views of the selected three protein conformations of the MurD enzyme used in virtual screening using multiple protein conformations. For clarity, the central and C-terminal domains are depicted in green. The C-terminal domain of selected MurD structures is depicted in three colors: yellow (1EEH–2UAG MurD intermediate structure), blue (1E0D–2UAG MurD intermediate structure), and red (2UAG MurD protein structure). (B) Calculated GRID contour surfaces of the hydrogen bond acceptor oxygen (O) probe (red) at -6.0 kcal/mol ; hydrogen bond acceptor nitrogen (N1) probe (blue) at -4.5 kcal/mol dry probe (green) at -0.5 kcal/mol and in the MurD binding site.

2. RESULTS AND DISCUSSION

2.1. Selection of MurD Protein Structures from TMD/OPS Simulations and Hot Spots Identification Using GRID Map Calculations. In the first step of our study, a selection of MurD protein structures for virtual screening experiments was performed. OPS energy studies suggested that energy demands connected with the C-terminal domain closing process confined to the same plane where both the N-terminal and central MurD domains are found to be energetically most favorable and thus also more available to the MurD enzyme.¹⁴ Further investigations of the off-path replica systems without included ligands demonstrated that in the 1E0D–2UAG replica system minimal energy is required for this large scale conformational change.¹⁴ The OPS 1EEH–2UAG graph in Figure 1 suggests that all conformational states on this closing pathway are readily accessible to the MurD enzyme indicating the existence of an equilibrium of easily available protein

structures between the free unbound and closed conformation of the enzyme.¹⁴ Following these data, a closed conformation of the MurD enzyme, corresponding to the closed 2UAG MurD structure, was selected as it relates to the lowest energy conformation on the investigated OPS energy landscape. In addition, two intermediate structures, one from 1E0D–2UAG and the other from 1EEH–2UAG trajectories, were selected. The intermediate structures represented the 35th replica of the OPS 1EEH–2UAG pathway (1EEH–2UAG MurD intermediate structure) and the 35th replica of the OPS 1E0D–2UAG pathway (1E0D–2UAG MurD intermediate structure). In both structures, the C-terminal domain was predominately located inside the plane of the N-terminal and C-terminal domains and, in terms of relative energy comparison, not far from the closed structure. The superimposed structures of selected MurD enzymes are depicted in two views in Figure 3A.

To further investigate the MurD ATP-binding sites in the selected protein structures and identify hot spots especially important for directing subsequent drug design, the GRID program²⁷ was utilized. GRID works by mapping the three-dimensional space around the investigated macromolecular targets with various probes, mimicking the chemical properties of most common atom types and small moieties to be found in ligands, thus enabling the identification of energetically favorable binding pots with desired characteristics.²⁷ As recommended in the literature, in order to design a suitable model all reported operations should be repeated using at least three different probes, namely the hydrophobic probe (DRY), hydrogen bond acceptor probe (O), and hydrogen bond donor probe (N1). Such a selection of probes allows a basic characterization of most interactions.²⁸

Selected three protein structures were used to obtain the energy contours for these three probes (DRY probe at -0.5 kcal/mol, O probe at -4.5 kcal/mol and N1 probe at -6.0 kcal/mol) that are presented in Figure 3B along with ATP molecule for better comparison. Only a minor hydrophobic region was identified by GRID mostly around the purine ATP moiety. From the GRID oxygen (O) contour surfaces at -6.0 kcal/mol, it can be clearly seen that two regions exist where the placement of hydrogen bond acceptor elements would be beneficial. First, a small area is located around the residue Asn271 where interaction with the purine of the ATP molecule takes place, and the second area is located where its phosphate groups interact with the protein.¹² Finally, the GRID nitrogen (N1) probe isolated two regions within the ATP-binding site, namely around Asn271 and the phosphate pocket, as possible placements of the hydrogen acceptor elements. Overall, the GRID results indicated that the molecule that could serve as an inhibitor in the ATP-binding pocket should include a hydrophobic element around the purine moiety, the Asn271 interaction and interactions within the phosphate part of the ATP-binding site.

2.2. Virtual Screening Procedure Combining LigandScout Structure-Based Pharmacophores with Molecular Docking Calculations. The LigandScout structure-based pharmacophore generator was used to derive²⁹ structure-based pharmacophores of the ATP molecule in the three selected MurD protein conformations, and observed interactions were carefully examined. Next, the initial number of pharmacophoric features used was reduced in all models to increase the chemical space identified by the pharmacophore model. In Figure 4A, the aligned two sets of LigandScout structure-based pharmacophores along with the ATP conformations are depicted.

The final models used in the large-scale virtual screening campaign were divided into two sets. All derived pharmacophore models included a hydrogen bond donor and a hydrogen bond acceptor feature mimicking the interaction between the ATP purine moiety and Asn271 observed in the 2UAG crystal structure, and a hydrophobic feature which was derived from the initially detected aromatic features of ATP purine moiety (Figure 4A). Exclusion volume spheres were included to take the spatial constraints of the ATP MurD protein binding site into account. One set of three structure-based pharmacophore models included these features and a negative ionizable feature generated by interpolating the negative ionizable pharmacophore elements detected by LigandScout in all three MurD conformations (Figure 4A, left). The other set of three pharmacophores included one magnesium binding feature

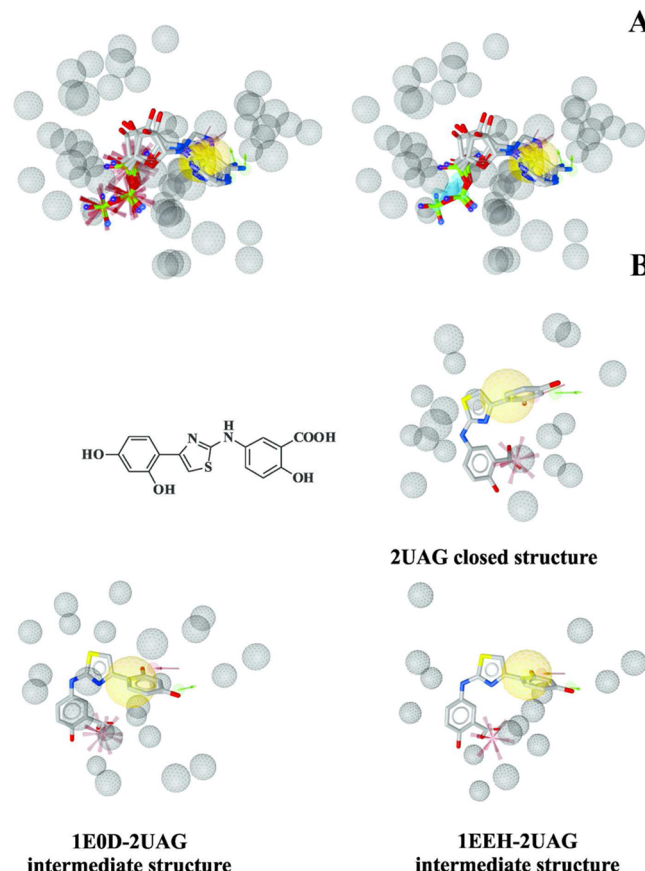


Figure 4. (A) Aligned LigandScout structure-based pharmacophores (left) with negative ionizable binding features, (right) with magnesium binding feature from three selected MurD protein structures. (B) Chemical structure of the hit compound 3 and conformations of the virtual hit 3 aligned to selected LigandScout structure-based pharmacophores using LigandScout as a screening engine. Green arrows represent hydrogen bond donors, red arrows hydrogen bond acceptors, and yellow spheres hydrophobic areas. Exclusion volume spheres (gray spheres) represent the derived spatial restraints of the MurD active site.

derived from the observed interactions of the ADP molecule with magnesium ion in the 2UAG structure (Figure 4A, right). The derived pharmacophores represent and reflect to a great extent the information from the GRID map calculations. In Figures 2S and 3S of the Supporting Information, the derived six pharmacophores without ligands are presented.

Subsequently, a large-scale virtual screening campaign was performed by screening our library of approximately 6.0 million commercially available compounds against six pharmacophore models with the LigandScout screening engine. This library of virtual compounds was prepared as described in the Materials and Methods section. The compounds were aligned to the investigated pharmacophore models using the alignment method available in the LigandScout program.^{29,30} The number of identified hits is shown in Table 1 (VS hits 1), and molecule 3 from the aminothiazole class identified as a hit is shown aligned to all three pharmacophores with included charged features in Figure 4B. Next, an example of hit molecule 8—a coumarin derivative—identified by the other set of three pharmacophores with a magnesium binding feature is shown in Figure 7S of the Supporting Information.

Table 1. Number of Virtual Hits from Each Performed Pharmacophore-Based Virtual Screening Campaign Using Sets of Three Pharmacophores^a

pharmacophore	phosphate LigandScout feature	VS hits 1	VS hits 2
2UAG MurD structure	negative ionizable feature	9026	913
	magnesium binding feature	38 008	900
1EEH–2UAG intermediate MurD structure	negative ionizable	5488	2941
	magnesium binding feature	28 668	10 721
1EOD–2UAG intermediate MurD structure	negative ionizable	3831	97
	magnesium binding feature	17 249	318

^a VS hits 1 represents the number of VS hits obtained by less restrictive exclusion volume coat around the six structure-based pharmacophores. VS hits 2 represents the number of VS hits obtained by more restrictive structure-based pharmacophores with an included additional exclusion volume coat based on the spatial restraints of the each studied MurD protein conformation.

The initially investigated six pharmacophore models yielded a considerable amount of hits from various chemical classes, ranging from 3831 to 38 008 virtual hits. In order to reduce the number of hits, we took the spatial constraint of the ATP-active site even more into account. Thus, in all six pharmacophore models, an additional more restrictive exclusion volume coat to limit the space around the molecule based on the spatial restraint of the MurD active site was defined (see Figures 2S and 3S in the Supporting Information for the derived new six pharmacophores from both sets with additional exclusion volume coat). A virtual screening campaign was performed again by screening our library of compounds against such new

restrictive sets of pharmacophores. The number of hits identified in this screening, shown again in Table 1 (VS hits 2), was now considerably decreased. However, in the 1EEH–2UAG protein structure where the C-terminal domain was located further away from the closed MurD conformation, the amount of virtual hits still remained large due to the conformational space available to the ligands.

The 97 and 318 virtual screening hits from the 1E0D–2UAG pharmacophores with restrictive exclusion volume coat were all visualized, and it was determined which of these hits were also identified in the remaining sets of pharmacophore searches. In addition, the uniformity of the alignments was assessed for the conformations of hits identified within the sets of pharmacophores. In the pharmacophore models with charged features, 46 compounds were found to be present in all pharmacophores with this feature, and the most unanimous distribution was observed for the aminothiazole derivatives, among them compounds 1–5. Identified compounds from other chemical classes included rhodanine or dihydropyrimidine-4,6-dione-based compounds with attached carboxylic functionality via various lipophilic spacers. In the case of pharmacophores with magnesium binding features, 186 compounds were present in all utilized pharmacophores. Several coumarin derivatives (e.g., compounds 8–10) were found to be present in all investigated pharmacophores with comparable alignment orientations (see Figure 7S of the Supporting Information for a pharmacophore-based alignment of the representative compound 8). In addition, compounds containing core thiazolopyridin-5-one or pyrimidin-4-ol moieties with similar substitutions as observed in compounds 8–10 showed potential in the performed screenings as well.

In the second stage of the virtual screening campaign, the 97 LigandScout hits obtained from the pharmacophore-based

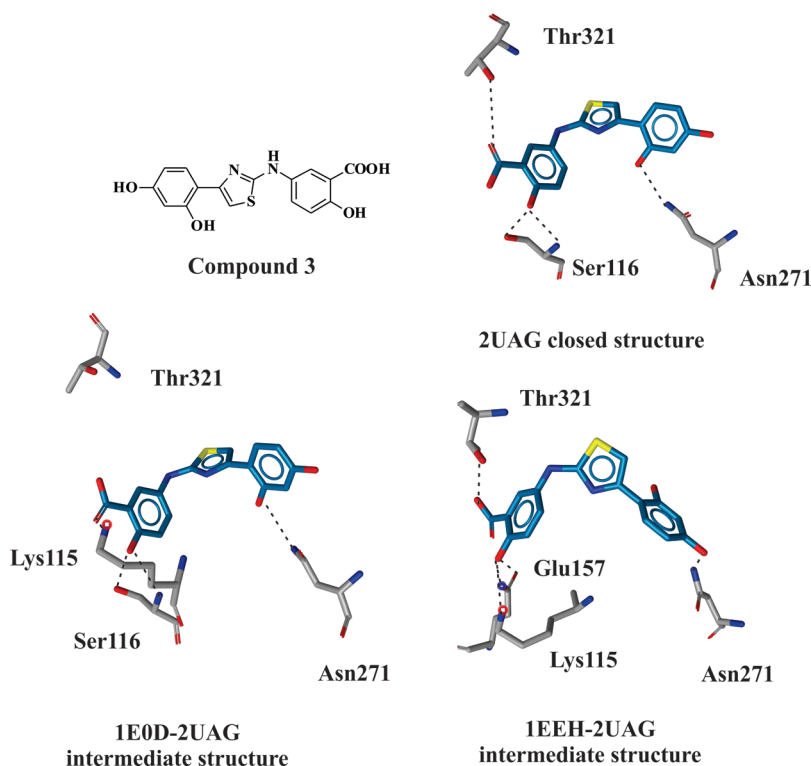


Figure 5. GOLD-calculated binding poses of the VS hit aminothiazole compound 3 docked into the ATP-binding site of the selected OPS/TMD MurD conformations, with depicted identified hydrogen bond interactions.

virtual screening campaigns with included negative ionizable features, and the 318 hits obtained from the screening with the incorporated magnesium binding feature, were docked into the ATP binding site of the three aforementioned MurD conformations using the GOLD molecular docking package.³¹ Active sites of the MurD conformations were prepared as described in the Materials and Methods section. The GOLDscore scoring function was used to assess the binding affinity of the calculated binding mode analogues (see Materials and Methods for more details).³² Obtained binding geometries were visually inspected for all hit compounds, and especially compounds present in all three searches were critically compared with respect to the uniformity of their binding modes and orientation obtained in the pharmacophore searches. This step of analysis represented the next criteria of compound selection. In Figure 5, GOLD-calculated binding poses of the hit aminothiazole compound 3 docked into the ATP-binding site of the selected MurD conformations are depicted along with the most important observed hydrogen bond interactions.

All conformations of compound 3 possessed a similar binding orientation, such as the ATP molecules within these structures (see Figure 6S for a comparison of the binding modes with the ATP molecule). When we investigated the interaction pattern for this compound, we established that it interacted predominately with two regions of the ATP-binding site. One interaction site is located in the vicinity of Asn271 which in the 2UAG crystal structure interacts with the 1H-purine part of the ATP molecule. Second, the carboxyl and hydroxyl groups on the attached benzene ring of 3 were found to interact with the regions of the binding site which normally interact with the phosphate groups of the ATP molecule. Predominantly, the 3-hydroxyl group at the benzene moiety of 3 formed most of the H-bond interactions with residues Ser114, Lys115, Ser116, and Glu157 located on the MurD central domain; in the 1EEH–2UAG intermediate and 2UAG MurD structures, compound 3 also interacted with Thr321 located on the C-terminal domain. The described interaction pattern thus entirely reflected the structure-based pharmacophore features that identified this molecule in the LigandScout virtual screening experiments. The remaining two classes of virtual hits identified in the pharmacophore-based virtual screening did not yield GOLD binding poses that were consistent throughout the three investigated MurD structures and were consequently not pursued experimentally.

The 318 hit compounds obtained from the virtual screening experiment from the second set of pharmacophores with the included magnesium binding feature were also docked into the three MurD conformations. The coumarin derivatives (e.g., compound 8–10) were the only class of compounds shown to be reproducing the GOLD binding modes most consistently with the same orientation mimicking the ATP molecule, while the docking modes of thiazolopyridin-5-ones or pyrimidin-4-ols were found to be less consistent. In Supporting Information Figure 8S, a comparison of the docking binding modes of coumarin compound 8 with the ATP molecule is shown. Two described classes of thiazole 1–5 and coumarin molecules 8–10 resulting from two diverse pharmacophore-based virtual screening campaigns showed the most promising behavior in terms of binding characteristics and consistency of the results at all levels of the multistep evaluation: similar pharmacophore alignment, docking pose consistency, and position of the compounds' interacting groups in accordance with the GRID

maps recommendations. Thus, these compounds have been selected for experimental evaluation. Compounds 6 and 7 from the thiazole series were additionally included to explore the influence of the carboxylic moiety.

Selected compounds 1–10 presented in Tables 1 and 2 (see Supporting Information for the origin of the compounds and

Table 2. Results of the Inhibition Assays of the Selected Aminothiazole Compounds 1–7 against *E. coli* MurC and MurD Ligases^a

Compound	R1	IC ₅₀ or RA (MurC)	IC ₅₀ or RA (MurD)
1		481 μM	84 %
2		681 μM	115 %
3		347 μM	555 μM
4		531 μM	98 %
5		81 %	98 %
6		90 %	95 %
7		83 %	97 %

^aResidual activities (RA) were determined at 100 μM of the compound.

for vendors' quality control procedures) were tested against MurD ligase and subsequently the remaining three enzymes of the ligase series MurC, MurE, and MurF, all originating from *E. coli*. To exclude possible nonspecific (promiscuous) inhibition, all compounds were tested in the presence of a detergent (0.005% Triton X-114).³³ It has to be noted that compounds 6 and 7 were included later in our study after the virtual screening procedure was already completed to further explore the SAR.

Compounds 1–7 represent aminothiazole derivatives linked directly to the 2,4-hydroxy-benzene moiety. The amino group of the aminothiazole ring is further substituted with various *meta* and/or *para* substituted phenyl moieties. From the selected set of compounds, only compound 3 with a 4-

carboxylic-3-hydroxyl substituted phenyl moiety was found to possess some MurD inhibition activity with an IC_{50} value of $555 \mu\text{M}$. Interestingly, the initial SAR information displayed very strict structural requirements for inhibition as the presence of only a carboxylic or hydroxyl group in compounds **1** and **5** resulted in a complete loss of inhibitory activity. Even reverse substitution of the hydroxyl/carboxylic pair on the benzene core in compound **2** resulted in a lack of MurD inhibitory activity. Compounds **6** and **7**, which were included to explore the influence of the carboxylic moiety, were found both as inactive.

Compounds **1–7** were also tested against the three other Mur ligases for potential multiple ligase inhibition due to observed similarities of the ATP-binding sites within the Mur ligase family.⁶ We were pleased to observe that compounds **1–4** were all found to possess MurC inhibitory activity with IC_{50} values of $481 \mu\text{M}$ (**1**), $681 \mu\text{M}$ (**2**), $347 \mu\text{M}$ (**3**), and $531 \mu\text{M}$ (**4**). On the remaining two enzymes, MurE and MurF, the compounds were rendered as inactive. Results of the inhibition values on the remaining Mur ligases are available in the Supporting Information in Table 3S. Compound **3** thus represents a new discovered dual inhibitor of *E. coli* MurC and MurD enzymes in a middle micromolar range. It has to be noted that for this class of compounds with the included aminothiazole moiety, inhibitory activity against bacterial DNA GyraseB was also established in the course of our previous work.³⁴

Next, compounds **8–10**, which represent selected 4-hydroxyl-5-chloro-coumarin derivatives with a substituted benzene moiety, were tested. Both parts were joined in the molecules by a flexible linker with an included rigid peptide bond element. These compounds, originating from the design strategy with an included magnesium binding feature, were found to be devoid of inhibitory activity against the MurD enzyme (Table 3). Further inhibition assays on MurC, MurE, and MurF did not reveal any inhibitory activity either (see Supporting Information Table 4S for obtained inhibition values).

Active compound **3** was tested for its *in vitro* antibacterial activity against three available bacterial strains: ATCC 29213 from *S. aureus*, ATCC 29212 from *E. faecalis*, and ATCC 49766

from *H. influenzae* using the protocol described in the Materials and Methods section. Cefuroxime and gentamicin were included as reference compounds. The results of the antibacterial testing are available in Table 4. Compound **3**

Table 4. In Vitro Antibacterial Activity (in $\mu\text{g}/\text{mL}$) of Selected Compound **3 and Reference Compounds**

compound	<i>S. aureus</i> ATCC 29213	<i>E. faecalis</i> ATCC 29212	<i>H. influenzae</i> ATCC 49766
3	128	>256	>256
cefuroxime	-	-	0.5
gentamicin	0.5	8	-

displayed a weak antibacterial activity against the bacterial strain ATCC 29213 from *S. aureus*. It is highly probable that the observed modest antibacterial activity of this compound is a result of the presence of the carboxylic group which in addition to several hydroxyl groups present in the molecule hinders the effective transport into the bacterial cell.

The obtained results were not optimal in terms of our expectation. Thus, we decided to further investigate them to provide an explanation for these rather low inhibition values that took a lot of structural as well as functional data into account. To begin with, in order to get more of a mechanistic insight into the inhibition mechanism of the newly discovered compounds, a steady-state kinetics study was performed for the most active compound **3** on the *E. coli* MurD enzyme with respect to the ATP substrate (see the Materials and Methods for details). In our previous work,¹⁸ the obtained apparent K_M values for each substrate ($K_{M,\text{app},\text{UMA}} = 6.0 \pm 0.8 \mu\text{M}$, $K_{M,\text{app},\text{D-Glu}} = 95 \pm 9 \mu\text{M}$, and $K_{M,\text{app},\text{ATP}} = 90 \pm 7 \mu\text{M}$) were fully in line with values reported in the literature for the MurD enzyme. After collecting results at different concentrations of ATP and compound **3** and fixed concentrations of UMA and D-Glu, the initial velocity data were fitted to competitive, noncompetitive, and uncompetitive (partial and full) inhibition models, and corresponding K_i values were calculated. The best statistical models are presented in Table 4, and Lineweaver–Burk plots are depicted in Figure 6.

Obtained results with the most reliable statistics ($R^2 = 0.884$) suggested the inhibition mechanism where compound **3** acts as a noncompetitive inhibitor with respect to ATP (Figure 6, Table 5). The K_i value of $587 \mu\text{M}$ determined for the partial noncompetitive model (Figure 6A) was in very good agreement with the IC_{50} result in the standard MurD screening assay ($IC_{50} = 555 \mu\text{M}$). The second model describing full noncompetitive inhibition with respect to ATP yielded similar statistics ($R^2 = 0.884$) but a higher K_i value of $693 \mu\text{M}$ compared to the IC_{50} value (Figure 6B). Currently, it is impossible to differentiate between both models and have a clear preference of one over the other. Finally, the third ranked model (Figure 6C) corresponds to competitive inhibition with respect to ATP. Despite comparable statistics ($R^2 = 0.887$) as in the previous cases, the determined K_i value of $87 \mu\text{M}$ was higher than the measured MurD IC_{50} inhibition value.

Noncompetitive inhibition is a type of enzyme inhibition where the inhibitor binds equally well to the enzyme whether or not it has already bound the investigated substrate, in the present case the ATP molecule. The steady-state kinetic results thus indicate that the inhibition of this compound is probably not taking place due to the direct competition of this compound with the ATP binding but rather through some

Table 3. Results of the Inhibition Assays of Selected Compounds **8–10 against *E. coli* MurD Ligase^a**

Compound	R1	RA % (MurD)
8		107 %
9		132 %
10		111 %

^aResidual activities (RA) were determined at $100 \mu\text{M}$ of the compound.

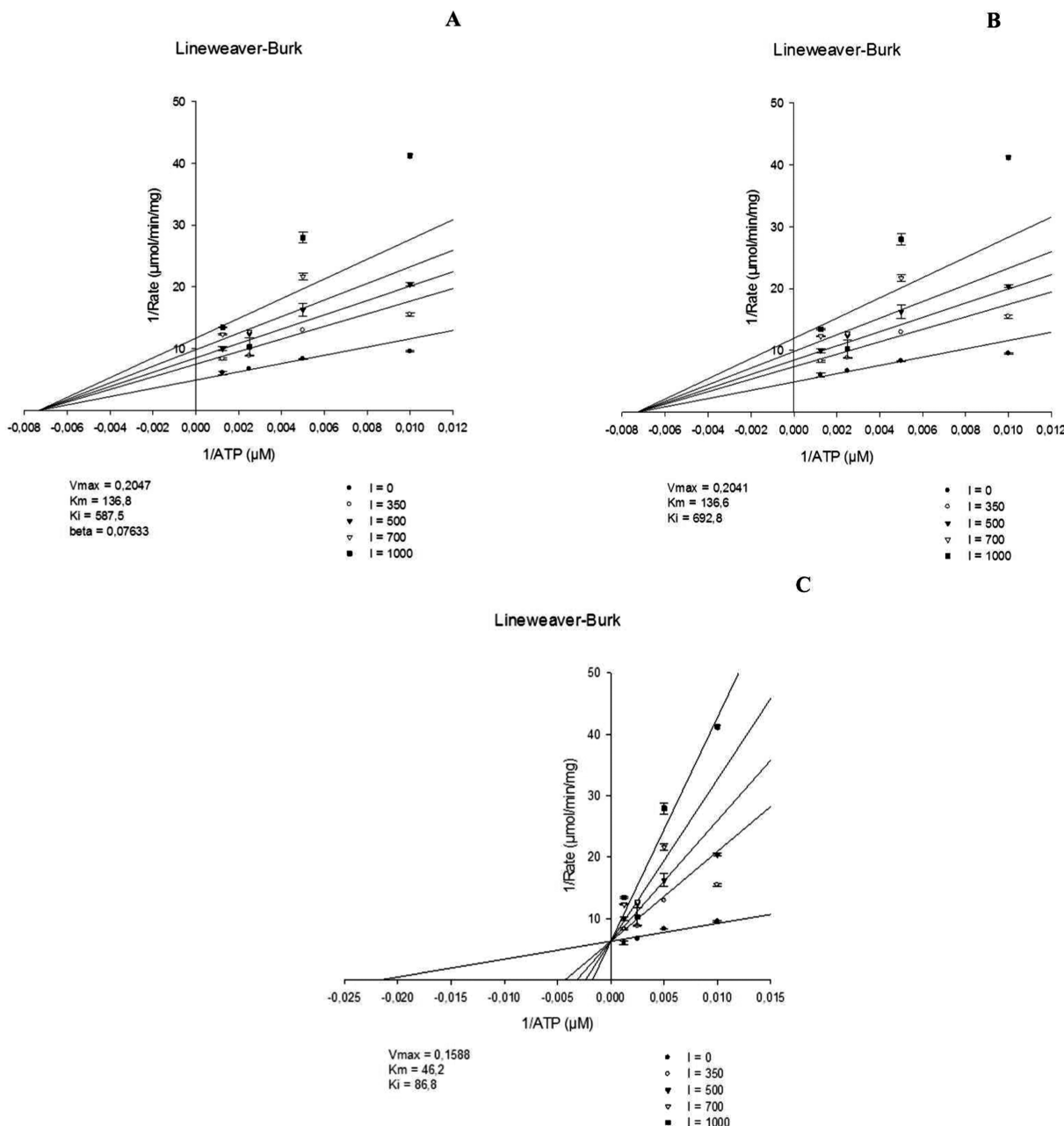
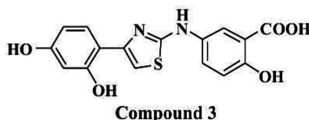


Figure 6. Lineweaver–Burk plots of the (A) partial and (B) full noncompetitive inhibition model and (C) competitive inhibition model of compound 3 versus ATP. Data were collected for compound 3 versus ATP and fixed concentrations of D-Glu (100 μ M) and UMA (80 μ M). For clarity, the data points shown are average values of the two data sets; the standard deviation was within $\pm 5\%$ of the average value.

Table 5. Data Collection and Inhibitory Properties of Compound 3 with Respect to ATP

substrate	inhibition mechanism	K_i (μ M)	global (shared) R^2
ATP	noncompetitive (partial)	587 μ M	0.884
ATP	noncompetitive (full)	693 μ M	0.884
ATP	competitive	87 μ M	0.874

mechanism where the ATP molecule is allowed to bind. It is important to note that although these observations offer some

important early insights into the binding of the aminothiazole class to the MurD enzyme, these observations cannot be directly transferred to binding properties of these compounds to other classes of Mur ligase enzymes. In addition, the observed conformational flexibility of the family⁶ poses an additional challenge to describe the positions from the available data. We will address these issues in our future studies.

To a certain degree, the observed MurC/MurD inhibition of compound 3 and the lack of MurE/MurF inhibition can be rationalized by the work reported by Smith⁶ based on structural

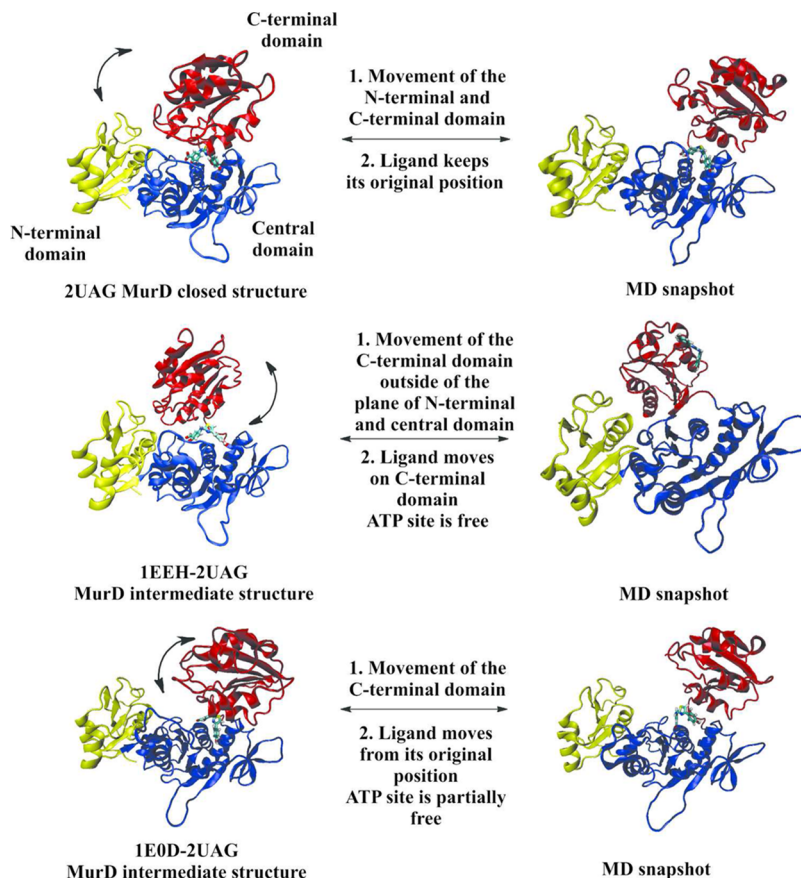


Figure 7. Structures of three MurD systems with docked compound 3 prepared for molecular dynamics (MD) simulation studies with a principal summary of the MD results. The N-terminal domain is colored in yellow, the central domain in blue, and the C-terminal domain in red. Before MD simulations, the MurD protein–ligand 3 systems were immersed into a TIP3 sphere of water molecules with truncated octahedral shape and the edge distance of 10 Å (for depiction of the MurD solvated systems, see Supporting Information, Figure 9S).

alignments of several structures within the Mur ligase family. It can be observed that the central domain is invariant in all ligases as this part of the molecule is responsible for binding of the ATP molecule while the two peripheral domains (C-terminal and N-terminal) display a considerable degree of flexibility and orientation to accommodate the two other substrates (UDP precursor and incoming amino acid or dipeptide). Smith observed a clear difference in the orientation of the N-terminal domain between the MurC/MurD pair of enzymes in contrast to the MurE/MurF pair, pointing to some extent toward a closer functional resemblance between both pairs of enzymes.⁶ We were interested as to whether this conformational flexibility of the peripheral domains can be a possible reason for the observed results. For this purpose, atomistic molecular dynamic simulation (MD) studies were initiated.

2.3. Molecular Dynamics (MD) Simulation Study of Aminothiazole Compound 3 in Complex with Selected TMD/OPS MurD Structures. In order to provide further insights into the dynamical behavior of the identified *E. coli* Mur ligase inhibitors and to potentially provide rationale for the observed experimental results, molecular dynamic (MD) simulations were initiated for the docked conformations of compound 3 in the ATP-binding sites of the three selected MurD conformations. Molecular dynamics (MD) calculations for the three investigated conformations of the MurD enzyme with the docked compound 3 were performed using the CHARMM molecular modeling suite,³⁵ thus the same force

field that was used in our previous TMD/OPS simulation studies.^{13,14} The three starting complexes are depicted in Figure 7. The CHARMM-GUI environment³⁶ was utilized for the protein manipulation and final construction of the solvated MurD compound 3 protein–ligand systems (for depiction of the MurD solvated systems, see the Supporting Information, Figure 9S). Following an equilibration procedure composed of two minimizations and a short MD simulation, 10 ns long production phase MD simulations were performed for all three systems. Observed dynamical behavior of the protein–ligand systems during the MD simulation runs can be observed also in the generated movie animations for each simulation (see the Supporting Information for the animations of each MD simulation).

The 10 ns production phase MD trajectories for the three MurD–compound 3 systems were subsequently analyzed in terms of geometrical parameters to identify protein domain mobility, especially the C-terminal and N-terminal domain. Thus, central domains of 5000 exported MD conformations for each simulated system were aligned to the initial conformation of the MurD central domain. Then, RMSD deviations of the N-terminal and C-terminal domains from the corresponding starting MurD structure for all three simulated cases were calculated. In Figure 8, RMSD time-dependent graphs are supplied for all three simulations, describing the general C-terminal and N-terminal protein domain movement with all heavy atoms taken into account.

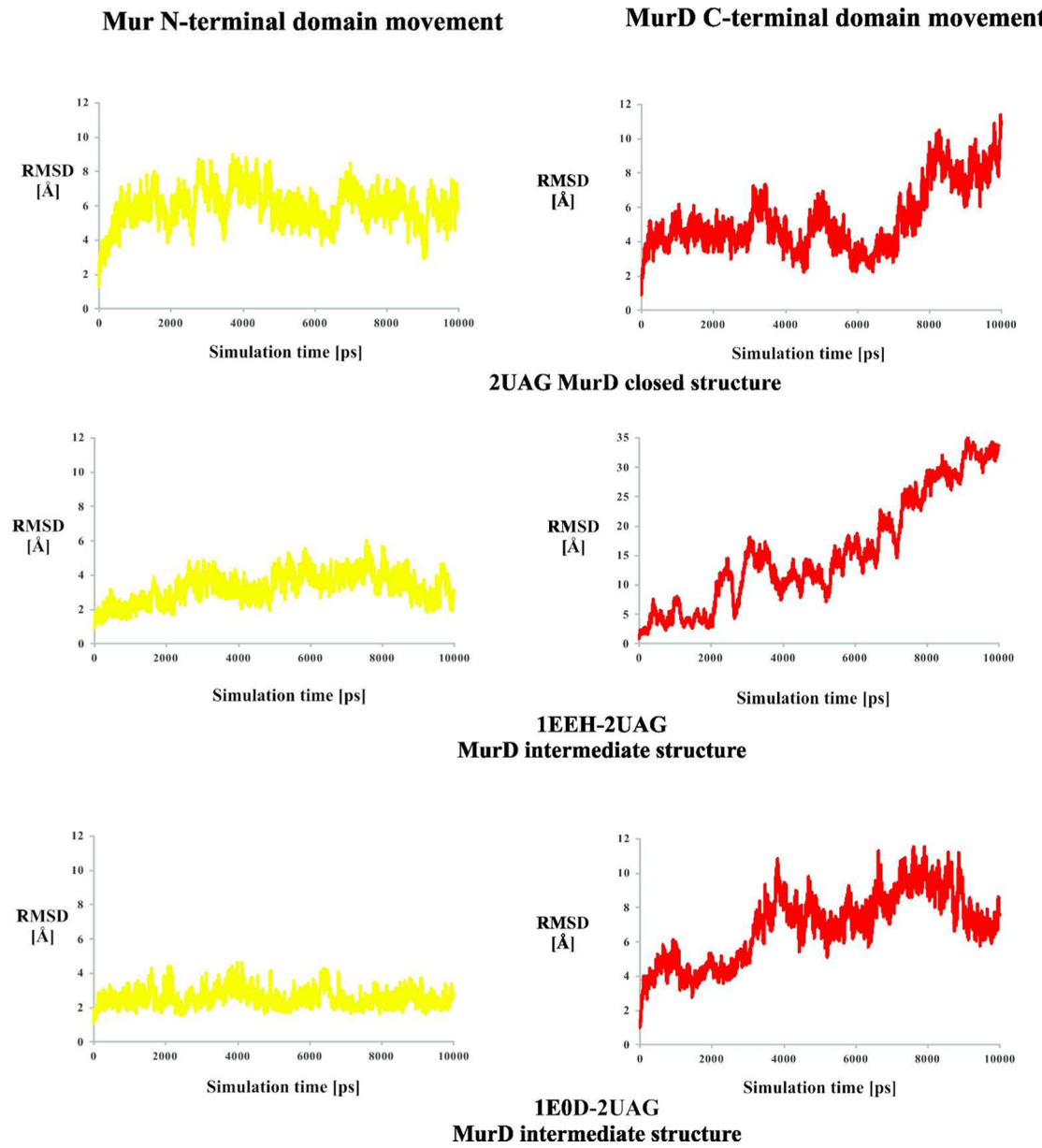


Figure 8. RMSD diagrams of the movements of the MurD enzyme N-terminal (left) and C-terminal (right) domain in complex with compound 3 for all three simulated cases—2UAG MurD structure, 1EEH–2UAG intermediate MurD structure, and 1E0D–2UAG intermediate MurD structure. Note that the RMSD axis for the graph describing the C-terminal domain movement for the 1EEH–2UAG MurD structure has a larger scale than the remaining graphs.

In all three cases, substantial domain movements of the N-terminal and C-terminal domain were observed relative to their initial OPS/TMD MurD positions. In the case of the simulated 2UAG MurD structure, which represents the boundary experimental MurD structure (PDB: 2UAG), its most pronounced protein domain movement was the motion of the N-terminal domain away from the closed conformation. In Figure 8, it can be observed how the overall RMSD of the N-terminal domain moves in the first nanoseconds of the MD simulation approximately 6 Å away from the initial position and then oscillates around this value. Next, after approximately 6.5 ns of the MD simulation, the motion of the C-terminal domain follows to the open conformation up to 11 Å away from the initial domain position. The bound compound 3 stays throughout the MD simulation in the vicinity of the docked conformation, interacting predominately with the central

domain and partially with the C-terminal domain, and does not overall alter its position considerably. For a better representation of the described protein domain motions, the corresponding 2UAG MurD MD animation is also provided. We would like to point out that such motions and mobility of the N-terminal domain have been documented experimentally for this family, especially for the MurC enzyme.⁶

Next, for the simulated 1EEH–2UAG intermediate MurD structure, the opening motion of the N-terminal domain was not observed to such a large extent as in the case of the 2UAG MurD structure, and this domain shifted only slightly away from the initial structure (observed RMSDs between 2 and 3 Å). On the other hand, the observed C-terminal domain movement was substantial in this conformation as it moved continuously from the initial conformation where the C-terminal domain is located in the same plane as the N-terminal

and central domains of MurD to a conformation where this domain was located outside of this plane (final RMSD difference of 35 Å). Note that the RMSD *y* axis for the graph describing the time-dependent C-terminal domain movement for the 1EEH–2UAG MurD structure has a larger scale than the remaining graphs in Figure 8. During the opening movement of the C-terminal domain, compound 3 stayed attached to the C-terminal domain and moved substantially away from its initial orientation. This leaves the ATP-binding site which is located predominately on the central domain free for the interaction with the substrate. For a better representation of the described domain motions, the corresponding 1EEH–2UAG MurD MD animation is provided in the Supporting Information.

Some observations from this MD simulation can be nicely compared with our steady-state kinetic results for compound 3. The performed MD simulation of the 1EEH–2UAG MurD structure without any introduced constraints in the water surroundings indicated the possibility of the existence of MurD conformations where the aminothiazole inhibitor is bound on the C-terminal domain and the ATP-binding site is left open for this interaction. Such conformations offer a potential explanation for the suggested noncompetitive inhibition kinetic models of compound 3, where the substrate (in our case ATP) and the inhibitor have no effect on the binding of the other and can bind and unbind the enzyme in either order. To some extent, it can also corroborate the observed lower IC₅₀ values. This example reveals the challenges that need to be addressed in drug design when trying to hit a flexible moving protein target²³ like, for example, our studied MurD enzyme and that even if we try to take the flexibility into account the outcomes can still be quite unpredictable due to the protein inherent flexibility which is not completely addressed.

Finally, for the 1E0D–2UAG intermediate MurD structure (see corresponding 1E0D–2UAG intermediate MurD MD animation), the opening motion of the N-terminal domain was considerably less pronounced as for the case of 2UAG MurD structure and the domain moved on average between 2 and 3 Å away from the initial structure. The C-terminal domain was found to move to the open conformation approximately 12 Å away for the initial domain position but still remained in the plain of central and N-terminal domains. The carboxylic and hydroxyl moieties of compound 3 preserved their interaction with the ATP-binding site, located on the central MurD domain. The resorcinol part of compound 3 no longer interacted with Asn271 and was in the course of the MD simulation relocated to interact with the C-terminal domain residues, leaving most of the ATP-binding site open to interact with the ATP molecule, in line with the observed steady-state kinetics results.

We would like to point out that protein motions with included ligands were also observed in the experiments on the MurD system, where a new open MurD conformation cocrystallized with an ATP analogue and UMA was solved, where the C-terminal domain is positioned in the plane of the N-terminal and central domains.³⁷ Our results complement and are in line with these observations and reveal even to a larger extent the great challenge that dynamic and highly flexible targets, Mur ligases, pose to computational structure-based drug design techniques.^{22,23}

3. CONCLUSION

The bacterial resistance of most of the available antibiotics underlines an urgent and unmet need for the discovery of novel efficacious antibacterial agents. In this study, we applied the results of our TMD/OPS simulation studies of the MurD C-terminal domain closing motion studies to the drug design application, namely, for the search for novel MurD ligase inhibitors by including the dynamical aspect of the C-terminal domain closing motion. Our main focus was the ATP-binding site of the MurD enzyme and design of potential inhibitors.

We designed a multistage design process to identify new inhibitors. In the first stage of the workflow, three protein MurD conformations were selected based on the obtained OPS/TMD energy data as the initial criterion. Next, the ATP-binding site in a different conformation was explored by GRID program identifying potential hot spots for the binding of hydrophobic and H-bond forming elements. Subsequently, a two-stage virtual screening approach was utilized, combining structure-based pharmacophores of the ATP molecule based on selected MurD conformations with molecular docking calculations using multiple protein structures. Selected compounds showing uniformity at all stages of screening were assayed in the established enzyme functional assays on all four Mur ligases (MurC–MurF), and compound 3 from the aminothiazole class was discovered to act as a dual MurC/MurD inhibitor in the middle micromolar range.

A steady-state kinetics study that was performed suggested that the compound acts as a noncompetitive inhibitor with respect to ATP. In the next stage, all utilized protein conformations of MurD with the included active compound 3 were subjected to molecular dynamics (MD) simulations to provide further dynamic insights into obtained experimental results. The results show the possibility of the existence of MurD conformations where the inhibitor is bound on the C-terminal domain of the MurD enzyme and the ATP-binding site is left open for this interaction, giving a structure-based explanation of the observed results and less potent inhibition values.

We aspire that this work, together with our dynamic models of binding and C-terminal domain movements of MurD,^{13,14} will contribute to a deeper understanding of these fascinating bacterial enzymes and supply novel information for advances in the design of novel antibacterials. In addition, this example underlines the challenges that need to be addressed when trying to hit a flexible moving target,^{22,23} such as for example the presently studied MurD bacterial enzyme.

4. MATERIALS AND METHODS

4.1. TMD and OPS Simulation Details and GRID Map Calculations.^{13,14} The TMD and OPS studies were performed as described in the corresponding refs 13 and 14 using the CHARMM molecular modeling suite³⁵ and a short summary is provided below. Experimentally determined open and closed structures of the MurD enzyme, which represented the starting coordinates for the Targeted Molecular Dynamics simulation studies (TMD),¹³ were retrieved from the Protein Data Bank using PDB entries: 2UAG (closed structure)⁷ and 1EEH and 1E0D (open structures) as boundary structures.¹⁰ The preparation and equilibration of the experimental MurD conformations as well as TMD simulation studies were designed, performed, and analyzed as described previously.¹³ The TMD simulation studies yielded two pathways of

conformational change using 2UAG and 1EEH (1EEH–2UAG trajectory) and 2UAG and 1E0D (1E0D–2UAG trajectory) structure pairs as boundary MurD conformations.¹³

To initiate off-path simulations (OPS), 50 equidistant replicas were prepared by extracting frames from the 1EEH–2UAG and 1E0D–2UAG TMD trajectories. The frames for the OPS calculations were sampled only in the part of the TMD trajectory where significant movement of the C-terminal domain can be observed.¹⁴ For each TMD system (1EEH–2UAG and 1E0D–2UAG) two pathways were computed, one with included ligands (UMA, ATP, and magnesium ions) and one with ligands removed. For each system composed of 50 replicas, 10^5 different pathways were calculated by an MD simulation under the off-path restraints. For the calculated pathways, work needed to move from one replica's orthogonal plane to the other during the conformational closure was calculated and analyzed.¹⁴ Three protein structures were selected for the virtual screening drug design application: 2UAG MurD structure (the final closed MurD structure), 1EEH–2UAG intermediate MurD structure (35 replica of the OPS 1EEH–2UAG pathway), and 1E0D–2UAG intermediate MurD structure (30 replica of the OPS 1EEH–2UAG pathway). For the three selected protein structures, GRID maps²⁷ were calculated for the ATP-binding site by using three conventional GRID molecular probes: hydrophobic probe (DRY), hydrogen bond acceptor probe (HBA) (O), and hydrogen bond donor probe (HBD) (N1). Such selection of probes allows a basic characterization of the most important interactions for subsequent drug design efforts.

4.2. Virtual Screening Campaign Using Multiple Protein Structures. **4.2.1. Structure-Based Pharmacophore Modeling and Pharmacophore-Based Virtual Screening Experiments Using Multiple MurD Protein Conformations.** The LigandScout structure-based pharmacophore generator was used in this part of our studies.²⁹ Structure-based pharmacophores were derived for the ATP conformation in three selected MurD protein conformation: 2UAG MurD structure, 1EEH–2UAG intermediate MurD structure, and 1E0D–2UAG intermediate MurD structure, and interactions were examined using the LigandScout software. Next, the initial number of pharmacophoric features was reduced in all models to increase the chemical space identified by the pharmacophore model. The final pharmacophore models used in the large-scale virtual screening campaign were divided into two sets of three pharmacophores. All six pharmacophore models included a hydrogen bond donor and a hydrogen bond acceptor feature mimicking the interaction between the ATP purine moiety and Asn271 observed in the 2UAG crystal structure and a hydrophobic feature which was derived from the initially detected aromatic features describing the purine ATP moiety. Exclusion volume spheres were included to take into account the spatial constraints of the ATP-binding site. One set of three structure-based pharmacophore models included all these features accompanied by an additional negative ionizable feature generated by interpolating negative ionizable features for the phosphate in all three structures. The other set of three pharmacophores included, instead of this feature, a magnesium binding feature derived by LigandScout between ADP and MurD enzyme in the 2UAG structure and MurD enzyme. All six pharmacophore models discussed so far were also represented with an additional exclusion volume coat based on the structural limitations of the ATP-binding site to further limit the space available to the molecule making all together 12

pharmacophore models (see Supporting Information, Figure 2S and 3S for the representation of less and more restrictive models used in virtual screening).

All models were screened against a library of approximately 6.0 million commercially available compounds, all of which were beforehand converted into multifunctional format (25 conformers for each compound in the database) using the LigandScout screening module. The conformers of the molecules in the screening library were generated using the idbgen module that is available in LigandScout, coupled with the OMEGA software.³⁸ The default high-throughput settings were used for the library generation: maximum number of output conformers per molecule = 25; RMS threshold to duplicate conformers = 0.8 Å; maximum number of all generated conformers per molecule = 30 000; and maximum number of intermediate conformers per molecule = 4000. In the virtual screening experiments, each compound had to fulfill all pharmacophore constraints to be identified as a virtual hit. The Pharmacophore Fit scoring function available in LigandScout was used to score the alignment of the hit molecules to the pharmacophore model.

4.2.2. Molecular Docking Calculations in Selected MurD Protein Conformations. Molecular docking calculations were performed using the GOLD³¹ molecular docking engine into three selected MurD protein conformations: 2UAG MurD structure, 1EEH–2UAG intermediate MurD structure, and 1E0D–2UAG intermediate MurD structure. Initial MD positions of the ATP molecules in all three investigated MurD protein conformations were used to define three binding sites taking all amino acids within the 10 Å radius into account. Each molecule was docked 10 times into the investigated binding site by applying the following parameters of the GOLD genetic algorithm (GA; population size = 100, selection pressure = 1.1, no. of operations = 100 000, no. of islands = 5, niche size = 2, migrate = 10, mutate = 95, crossover = 95). Early termination was allowed if the top three solutions were within 1.5 Å of the RMSD value. The quality of the generated binding poses as well as scoring function assessment³² were performed first by redocking the ADP molecule into the 2UAG MurD crystal structure using the GOLDScore and ChemScore scoring function. A better reproduction was established when using the GOLDscore scoring function which was used in all remaining docking calculations (see Supporting Information, Figure 4S for comparison of the GOLDscore and CHEMScore generated ADP binding mode with the X-ray conformation). Next, three ATP molecules were redocked into three corresponding selected MurD protein conformations, and a comparison was made with the initial conformations (see Supporting Information, Figure 5S for conformation of the binding modes). In all three cases, a good reproduction of the binding modes was observed. Obtained LigandScout virtual screening hits were docked into the defined MurD ATP-binding sites of three selected structures using GOLD with the settings described above. The GOLDscore scoring function was used to assess the affinity of the produced complexes in all investigated cases.

4.3. Biological assays of *E. coli* Mur Ligase Inhibition (All MurC-MurF). Inhibition Assay. The inhibition of Mur ligases was determined using the Malachite green assay with slight modifications.^{39,40} The mixture with a final volume of 50 μL contained

MurC. 50 mM Hepes, pH 8.0, 5 mM MgCl₂, 0.005% Triton X-114, 120 μM L-Ala, 120 μM UMP, 450 μM ATP, purified

MurC from *E. coli*, and 100 μM of each tested compound dissolved in DMSO.

MurD. 50 mM Hepes, pH 8.0, 5 mM MgCl₂, 0.005% Triton X-114, 100 μM d-Glu, 80 μM UMA, 400 μM ATP, purified MurD from *E. coli*, and 100 μM of each tested compound dissolved in DMSO.

MurE. 50 mM Hepes, pH 8.0, 15 mM MgCl₂, 0.005% Triton X-114, 60 μM mDAP, 100 μM UMAG, 1000 μM ATP, purified MurE from *E. coli*, and 100 μM of each tested compound dissolved in DMSO.

MurF. 50 mM Hepes, pH 8.0, 50 mM MgCl₂, 0.005% Triton X-114, 600 μM d-Ala-d-Ala, 100 μM UMtri-mDAP, 500 μM ATP, purified MurF from *E. coli*, and 100 μM of each tested compound dissolved in DMSO.

In all cases, the final concentration of DMSO was 5% (v/v). After incubation for 15 min at 37 °C, the enzyme reaction was terminated by adding Biomol reagent, and the absorbance was measured at 650 nm. All experiments were run in duplicate. Residual activities (RAs) were calculated with respect to similar assays without the tested compounds and with 5% DMSO. The IC₅₀ values, which were determined by measuring the residual activities at seven different compound concentrations, represented the concentration for which the RA was 50%. Compound 3 from the discovered class of inhibitors was characterized by NMR, and its purity was determined by microanalysis performed on a PerkinElmer C, H, N, S analyzer using a modified Pregl–Dumas method. The purity of the tested compound was established to be $\geq 95\%$ (see Supporting Information, section 2).

4.4. Kinetic Analysis of Compound 3 Binding to MurD.

For compound 3, K_i values were determined from MurD *E. coli* inhibition. K_i determination was performed under similar conditions as described for the MurD inhibition assay,^{39,40} where a different concentration of one substrate (ATP) and fixed concentration of the other two (d-Glu and UMA) were used. The concentration of ATP (100, 200, 400, and 800 μM) was varied at a fixed concentration of UMA (80 μM) and d-Glu (100 μM). The concentrations of 3 were 0, 350, 500, 700, and 1000 μM . After 15 min of incubation, 100 μL of Biomol green reagent was added, and the absorbance was read at 650 nm after 5 min. Initial velocity data were fitted to competitive, noncompetitive, and uncompetitive inhibition models using SigmaPlot 12.0 software, and K_i values were calculated for the best fitted models.

4.5. Determination of Antibacterial Activity of Compound 3. The antibacterial activity study for compound 3 was performed at the Department of Microbiological Surveillance and Research, Statens Serum Institute in Copenhagen, Denmark. Fresh overnight colonies from 5% horse blood agar plates (*Staphylococcus aureus* and *Enterococcus faecalis*) or chocolate agar plates (*Haemophilus influenzae*) were suspended to a turbidity of 0.5 McFarland and further diluted 1:100 in Mueller-Hinton (MH) (*S. aureus* and *E. faecalis*) or *Haemophilus* Test Medium (HTM) broth. Stock solution of the tested compound was prepared in DMSO, and stock solutions of standards (gentamicin, cefuroxime) were prepared in sterile water. All microtiter plates had added 50 μL of MH/DMSO (*S. aureus* and *E. faecalis*) or HTM/DMSO (*H. influenzae*). For control compounds, only broth without DMSO was added. 50 μL of relevant solutions was added to the first row and then diluted 1:1. A total of 50 μL of diluted bacterial suspension was added to wells containing 50 μL of 2-fold compound dilutions. The test range was 0.25–256 $\mu\text{g}/\text{mL}$. The plates were

incubated at 35 °C in ambient air for 16–20 h for *S. aureus* and *E. faecalis* and 20–24 h for *H. influenzae*. Colony counts of the used inoculum were correct, namely 1 $\times 10^6$ CFU/mL, and all control compounds were within the limits according to CLSI. Control of DMSO for *S. aureus*, *E. faecalis*, and *H. influenzae* growth were seen in all wells indicating the concentration of DMSO had no influence of the growth of the bacteria. All experiments were performed in triplicate, and the results, MIC in $\mu\text{g}/\text{mL}$, are shown in Table 4.

4.6. Molecular Dynamics (MD) Simulation Studies of Three MurD Complexes with Compound 3. Molecular dynamics (MD) calculations for the three investigated conformations of the MurD enzyme 2UAG MurD structure, 1EEH–2UAG intermediate MurD structure, and 1E0D–2UAG intermediate MurD structure with corresponding docked conformations of the compound 3 were performed using the CHARMM molecular modeling suite.³⁵ The bound conformations of inhibitor 3 in three conformations of the MurD ATP-binding site—initials starting points for the MD simulations—were generated as described in section 4.2 using the GOLD molecular docking suite. The CHARMM-GUI environment was utilized for the protein manipulation and construction of the solvated MurD protein-compound 3 system.³⁶ CHARMM parameter and topology files (version 27) were utilized to specify the force field parameters of the amino acid residues comprising the MurD protein.^{41,42} The CHARMM General Force Field (CGenFF) was used to describe the atom types and partial charges of compound 3.⁴³ Determined partial charges and assigned atom types for compound 3 are listed in the Supporting Information (see Table S5). Carbamylated lysine residue 198 (KCX198) found in the MurD enzyme was, as it was located considerably far away from the bound conformation of 3, modeled as a lysine residue. The new structural results showed that such a configuration of the this residue can also be determined experimentally.³⁷ The MurD protein ligand systems were immersed into a sphere of TIP3 water molecules⁴⁴ with truncated octahedral shape with the edge distance of 10 Å, and 16 potassium ions were added to each system to make it electroneutral (see Supporting Information Figure 9S for solvated three MurD ligand 3-protein complexes). Ion placement was performed using the Monte Carlo method. The periodic boundary conditions (PBC) were applied based on the shape and size system, and Fast Fourier Transform (FFT) grid information on the Particle-mesh Ewald (PME) method was determined. The final systems for MD simulation were composed of 44 402 atoms (2UAG MurD structure), 44 453 atoms (1EEH–2UAG intermediate MurD structure), and 49 208 atoms (1E0D–2UAG intermediate MurD structure). Short steps of energy minimization were then performed to remove bad contacts. Three systems were then minimized for 2000 steps using the steepest descent (SD) method followed by 2000 steps of the modified Adopted Basis Newton–Raphson (ABNR) method and an MD equilibration run of 350 ps.

Production MD trajectories were generated using the leapfrog integration scheme and 2 fs simulation step using the SHAKE algorithm. Ten-nanosecond-long MD simulation production runs were performed. Conformations were sampled every 100th step resulting in 5000 conformations for subsequent analysis. Visualization and analysis of the geometry parameters (atom distances, RMS fluctuations, etc.) of the production MD trajectories were performed using the VMD program.^{45,46} Further inspection of the overall conformational

behavior for each MD simulation can also be seen in the generated movie animations (see Supporting Information movies 1EEH–2UAG structure, 1E0D–2UAG structure, and 2UAG structure).

■ ASSOCIATED CONTENT

§ Supporting Information

(1) Complete list of assayed compounds, (2) analytical and spectral characterization data of active compound 3, (3) OPS energy diagrams of two TMD-generated closing motions of the MurD C-terminal domain with included ligands, (4) derived structure-based pharmacophores of the ATP interaction pattern based on three selected TMD/OPS MuD protein conformations, (5) GOLD molecular docking tool validation and docking in three selected TMD/OPS MurD protein conformations, (6) visualization of the virtual screening experiments—additional features, (7) results of the biological assay of selected compounds against MurC-MurF ligases, (8) partial charges and atoms types for simulated compound 3, (9) solvated systems of GOLD-generated binding mode of compound 3 in three different conformations of MurD enzyme. Animation movies of each performed MD simulation. This material is available free of charge via the Internet at <http://pubs.acs.org>.

■ AUTHOR INFORMATION

Corresponding Author

*Phone: +386-1-4760-376. Fax: +386-1-4760-300. E-mail: andrej.perdih@ki.si.

Notes

The authors declare no competing financial interest.

■ ACKNOWLEDGMENTS

This work was supported by the Ministry of Higher Education, Science and Technology of the Republic of Slovenia (postdoctoral grant number: Z1-4111). Dr. Andreja Kovač from the Faculty of Pharmacy, University of Ljubljana, is acknowledged and thanked for performing initial inhibition assays of some of the novel compounds discussed in this work. Dr. Yasmin Aristei from Molecular Discovery Ltd. is thanked for GRID map calculations. Dr. Didier Blanot from the Université Paris-Sud, Orsay, France is thanked for critical reading of the manuscript.

■ REFERENCES

- (1) Silver, L. L. Does the cell wall of bacteria remain a viable source of targets for novel antibiotics? *Biochem. Pharmacol.* **2006**, *71*, 996–1005.
- (2) Brown, E. D.; Wright, G. D. New Targets and Screening Approaches in Antimicrobial Drug Discovery. *Chem. Rev.* **2005**, *105*, 759–774.
- (3) Silver, L. L. Challenges of Antibacterial Discovery. *Clin. Microbiol. Rev.* **2011**, *24*, 71–109.
- (4) Vollmer, W.; Blanot, D.; de Pedro, M. A. Peptidoglycan structure and architecture. *FEMS Microbiol. Rev.* **2008**, *32*, 149–167.
- (b) Barreteau, H.; Kovač, A.; Boniface, A.; Sova, M.; Gobec, S.; Blanot, D. *FEMS Microbiol. Rev.* **2008**, *32*, 168–207. (c) Sink, R.; Barreteau, H.; Patin, D.; Mengin-Lecreux, D.; Gobec, S.; Blanot, D. *BioMol. Concepts* **2013**, *4*, 539–546.
- (5) van Heijenoort, J. Recent advances in the formation of the bacterial peptidoglycan monomer unit. *Nat. Prod. Rep.* **2001**, *18*, 503–519.
- (6) Smith, C. S. Structure, Function and Dynamics in the mur Family of Bacterial Cell Wall Ligases. *J. Mol. Biol.* **2006**, *362*, 640–655.
- (7) Bertrand, J. A.; Auger, G.; Martin, L.; Fanchon, E.; Blanot, D.; Le Beller, D.; van Heijenoort, J.; Dideberg, O. Determination of the MurD mechanism through crystallographic analysis of enzyme complexes. *J. Mol. Biol.* **1999**, *289*, 579–590.
- (8) Perdih, A.; Hodosek, M.; Solmajer, T. MurD ligase from *E. coli*: Tetrahedral intermediate formation study by hybrid quantum mechanical/molecular mechanical replica path method. *Proteins* **2009**, *74*, 744–759.
- (9) Anderson, M. S.; Eveland, S. S.; Onishi, H.; Pompiano, D. L. Kinetic mechanism of the *Escherichia coli* UDPMurNAc-tripeptide D-alanyl-D-alanine-adding enzyme: use of a glutathione S-transferase fusion. *Biochemistry* **1996**, *35*, 16264–16269.
- (10) Emanuele, J. J., Jr.; Jin, H.; Yanchunas, J., Jr.; Villafranca, J. J. Evaluation of the kinetic mechanism of *Escherichia coli* uridine diphosphate-N-acetylmuramate:L-alanine ligase. *Biochemistry* **1997**, *36*, 7264–7271.
- (11) Bouhss, A.; Dementin, S.; van Heijenoort, J.; Parquet, C.; Blanot, D. MurC and MurD synthetases of peptidoglycan biosynthesis: Borohydride trapping of acyl-phosphate intermediates. *Methods Enzymol.* **2002**, *354*, 189–196.
- (12) Bertrand, J. A.; Fanchon, E.; Martin, L.; Chantalat, L.; Auger, G.; Blanot, D.; van Heijenoort, J.; Dideberg, O. “Open” structures of MurD: domain movements and structural similarities with folylpolyglutamate synthetase. *J. Mol. Biol.* **2000**, *301*, 1257–1266.
- (13) Perdih, A.; Kotnik, M.; Hodosek, M.; Solmajer, T. Targeted Molecular Dynamics Simulation Studies of Binding and Conformational Changes in *E.Coli* MurD. *Proteins* **2007**, *68*, 243–254.
- (14) Perdih, A.; Solmajer, T. MurD ligase from *E.coli*: C-terminal domain closing motion. *Comput. Theor. Chem.* **2012**, *979*, 73–81.
- (15) Zoebiy, A. E.; Sanschagrin, F.; Levesque, R. C. Structure and function of the Mur enzymes: Development of novel Inhibitors. *Mol. Microbiol.* **2002**, *47*, 1–12.
- (16) Perdih, A.; Kovač, A.; Wolber, G.; Blanot, D.; Gobec, S.; Solmajer, T. Discovery of novel benzene 1,3-dicarboxylic acid inhibitors of bacterial MurD and MurE ligases by structure-based virtual screening approach. *Bioorg. Med. Chem. Lett.* **2009**, *19*, 2668–2673.
- (17) Tanner, M. E.; Vaganay, S.; van Heijenoort, J.; Blanot, D. Phosphinate Inhibitors of the D-Glutamic Acid-Adding Enzyme of Peptidoglycan Biosynthesis. *J. Org. Chem.* **1996**, *61*, 1756–1760.
- (18) Kotnik, M.; Humljan, J.; Contreras-Martel, C.; Oblak, M.; Kristan, K.; Hervé, M.; Blanot, D.; Urleb, U.; Gobec, S.; Dessen, A.; Solmajer, T. Structural and Functional Characterization of Enantiomeric Glutamic Acid Derivatives as Potential Transition State Analogue Inhibitors of MurD Ligase. *J. Mol. Biol.* **2007**, *370*, 107–115.
- (19) Perdih, A.; Bren, U.; Solmajer, T. Binding Free-Energy Calculations of N-Sulfonyl Glutamic Acid Inhibitors of MurD Ligase. *J. Mol. Model.* **2009**, *15*, 983–996.
- (20) Perdih, A.; Wolber, G.; Solmajer, T. Molecular dynamics simulation and linear interaction energy study of D-Glu-based inhibitors of the MurD ligase. *J. Comput.-Aided Mol. Des.* **2013**, *27*, 723–738.
- (21) (a) Tomašić, T.; Kovač, A.; Klebe, G.; Blanot, D.; Gobec, S.; Kikelj, D.; Mašić, L. P. Virtual screening for potential inhibitors of bacterial MurC and MurD ligases. *J. Mol. Model.* **2012**, *18*, 1063–1072. (b) Šink, R.; Kovač, A.; Tomašić, T.; Rupnik, V.; Boniface, A.; Bostock, J.; Chopra, I.; Blanot, D.; Masic, L. P.; Gobec, S.; Zega, A. Synthesis and biological evaluation of N-acylhydrazones as inhibitors of MurC and MurD ligases. *ChemMedChem* **2008**, *9*, 1362–1370.
- (22) Carlson, H. A. Protein flexibility and drug design: how to hit a moving target. *Curr. Opin. Chem. Biol.* **2002**, *4*, 447–452.
- (23) Teague, S. J. Implications of protein flexibility for drug discovery. *Nat. Rev. Drug Discovery* **2003**, *2*, 527–541.
- (24) Knegtel, R. M.; Kuntz, I. D.; Oshiro, C. M. Molecular docking to ensembles of protein structures. *J. Mol. Biol.* **1997**, *266*, 424–440.
- (25) Meagher, K. L.; Carlson, H. A. Incorporating protein flexibility in structure-based drug discovery: using HIV-1 protease as a test case. *J. Am. Chem. Soc.* **2004**, *126*, 13276–13281. (b) Kunze, J.; Todoroff, T.; Schneider, P.; Rodrigues, T.; Geppert, T.; Reisen, F.; Schreuder,

- H.; Saas, J.; Hessler, G.; Baringhaus, K.-G.; Schneider, G. Targeting Dynamic Pockets of HIV-1 Protease by Structure-Based Computational Screening for Allosteric Inhibitors. *J. Chem. Inf. Model.* **2014**, *54*, 987–991.
- (26) Longenecker, K. L.; Stamper, G. F.; Hajduk, P. J.; Fry, E. H.; Jakob, C. G.; Harlan, J. E.; Edalji, R.; Bartley, D. M.; Walter, K. A.; Solomon, L. R.; Holzman, T. F.; Gu, Y. G.; Lerner, C. G.; Beutel, B. A.; Stoll, V. S. Structure of MurF from *Streptococcus pneumoniae* co-crystallized with a small molecule inhibitor exhibits interdomain closure. *Protein Sci.* **2005**, *14*, 3039–3047.
- (27) Goodford, P. J. A computational procedure for determining energetically favorable binding sites on biologically important macromolecules. *J. Med. Chem.* **1985**, *28*, 857–864.
- (28) Ortuso, F.; Langer, T.; Alcaro, S. GBPM: GRID-based pharmacophore model: concept and application studies to protein-protein recognition. *Bioinformatics* **2006**, *22*, 1449–1455.
- (29) Wolber, G.; Langer, T. LigandScout: 3-D Pharmacophores Derived from Protein-Bound Ligands and Their Use as Virtual Screening Filters. *J. Chem. Inf. Model.* **2005**, *45*, 160–169.
- (30) Wolber, G.; Dornhofer, A.; Langer, T. Efficient overlay of small organic molecules using 3D pharmacophores. *J. Comput.-Aided Mol. Des.* **2006**, *20*, 773–788.
- (31) Jones, G.; Willett, P.; Glen, R. C.; Leach, A. R.; Taylor, R. Development and validation of a genetic algorithm for flexible docking. *J. Mol. Biol.* **1997**, *267*, 727–748.
- (32) Kirchmair, J.; Markt, P.; Distinto, S.; Wolber, G.; Langer, T. Evaluation of the performance of 3D virtual screening protocols: RMSD comparisons, enrichment assessments, and decoy selection - what can we learn from earlier mistakes? *J. Comput.-Aided Mol. Des.* **2008**, *22*, 213–228.
- (33) McGovern, S. L.; Stoichet, B. K. Kinase inhibitors: not just for kinases anymore. *J. Med. Chem.* **2003**, *46*, 1478–1483.
- (34) Brvar, M.; Perdih, A.; Oblak, M.; Peterlin Masic, L.; Solmajer, T. In silico discovery of 2-amino-4-(2,4-dihydroxyphenyl)thiazoles as novel inhibitors of DNA gyrase B. *Bioorg. Med. Chem. Lett.* **2010**, *20*, 958–962.
- (35) Brooks, B. R.; Bruccoleri, R. E.; Olafson, B. D.; States, D. J.; Swaminathan, S.; Karplus, M. CHARMM: A Program for Macromolecular Energy, Minimization, and Dynamics Calculations. *J. Comput. Chem.* **1983**, *4*, 187–217.
- (36) Jo, S.; Kim, T.; Iyer, V. G.; Im, W. CHARMM-GUI: A web-based graphical user interface for CHARMM. *J. Comput. Chem.* **2008**, *29*, 1859–1865.
- (37) Šink, R.; Kotník, M.; Barreteau, H.; Zega, A.; Gobec, S.; Blanot, D.; Dessen, A.; Contreras-Martel, C. Conformational insights into a rigid body C-terminal domain movement of MurD ligase. *Drugs Future* **2010**, *35* (Suplement A), PC257, 170.
- (38) (a) OMEGA 2.4.6; OpenEye Scientific Software, Inc.: Santa Fe, NM, <http://www.eyesopen.com>. (b) Hawkins, P. C. D.; Skillman, A. G.; Warren, G. L.; Ellingson, B. A.; Stahl, M. T. Conformer generation with OMEGA: Algorithm and validation using high quality structures from the protein databank and the Cambridge structural database. *J. Chem. Inf. Model.* **2010**, *50*, 572–584.
- (39) Auger, G.; Martin, L.; Bertrand, J.; Ferrari, P.; Fanchon, E.; Vaganay, S.; Petillot, Y.; van Heijenoort, J.; Blanot, D.; Dideberg, O. Large-scale preparation, purification, and crystallization of UDP-N-acetylmuramoyl-L-alanine: D-glutamate ligase from *Escherichia coli*. *Prot. Express Purif.* **1998**, *13*, 23–29.
- (40) Lanzetta, P. A.; Alvarez, L. J.; Reinach, P. S.; Candia, O. An improved assay for nanomole amounts of inorganic phosphate. *Anal. Biochem.* **1979**, *100*, 95–97.
- (41) MacKerell, A. D., Jr.; Bashford, D.; Bellott, M.; Dunbrack, R. L., Jr.; Evanseck, J. D.; Field, M. J.; Fischer, S.; Gao, J.; Guo, H.; Ha, S.; Joseph-McCarthy, D.; Kuchnir, L.; Kuczera, K.; Lau, F. T. K.; Mattos, C.; Michnick, S.; Ngo, T.; Nguyen, D. T.; Prodhom, B.; Reiher, W. E., III; Roux, B.; Schlenkrich, M.; Smith, J. C.; Stote, R.; Straub, J.; Watanabe, M.; Wiorkiewicz-Kuczera, J.; Yin, D.; Karplus, M. All-atom empirical potential for molecular modeling and dynamics Studies of proteins. *J. Phys. Chem. B* **1998**, *102*, 3586–3616.
- (42) MacKerell, A. D., Jr.; Feig, M.; Brooks, C. L., III. Extending the treatment of backbone energetics in protein force fields: limitations of gas-phase quantum mechanics in reproducing protein conformational distributions in molecular dynamics simulations. *J. Comput. Chem.* **2004**, *25*, 1400–1415.
- (43) Vanommeslaeghe, K.; Hatcher, E.; Acharya, C.; Kundu, S.; Zhong, S.; Shim, J.; Darian, E.; Guvench, O.; Lopes, P.; Vorobyov, I.; Mackerell, A. D., Jr. CHARMM general force field: A force field for drug-like molecules compatible with the CHARMM all-atom additive biological force fields. *J. Comput. Chem.* **2010**, *671*–690.
- (44) Jorgensen, W. L.; Chandrasekhar, J.; Madura, J. D.; Impey, R. W.; Klein, M. L. Comparison of simple potential functions for simulating liquid water. *J. Chem. Phys.* **1983**, *79*, 926–935.
- (45) Humphrey, W.; Dalke, A.; Schulten, K. VMD: visual molecular dynamics. *J. Mol. Graphics* **1996**, *14*, 33–38.
- (46) Frishman, D.; Argos, P. Knowledge-based protein secondary structure assignment. *Proteins* **1995**, *23*, 566–579.